A manifestation of the Ostwald step rule: Molecular-dynamics simulations and free-energy landscape of the primary nucleation and melting of single-molecule polyethylene in dilute solution

L. Larini and D. Leporini*

Dipartimento di Fisica "Enrico Fermi",

Università di Pisa,

Largo B.Pontecorvo 3,

I-56127 Pisa, Italy

and

INFM-CRS SOFT,

Largo B.Pontecorvo 3,

I-56127 Pisa, Italy

(Dated: September 3, 2008)

Abstract

The paper presents numerical results from extensive MD simulations of the crystallization process of a single polyethylene chain with $N = 500$ monomers. The development of the ordered structure is seen to proceed along different routes involving either the global reorganization of the chain or, alternatively, well-separated connected nuclei. No dependence on the thermal history was observed at the late stages of the crystallization. The folding process involves several intermediate ordered metastable states, in strong analogy with the experiments, and ends up in a well-defined long-lived lamella with ten stems of approximately equal lenght, arranged into a regular, hexagonal pattern. This behaviour may be seen as a *microscopic* manifestation of the Ostwald step rule. Both the metastable states and the long-lived one are evidenced as the local minima and the global one of the free-energy landscape (FEL), respectively. The study of the microscopic organization of the lamella evidenced that the two caps are rather flat, i.e. the loops connecting the stems are short. Interestingly, annealing the chain through the different metastable states leaves the average number of monomers per loop nearly unchanged. It is also seen that the chain ends, the so-called cilia, are localized on the surface of the lamella, in agreement with the experiments, and that structural fluctuations take place on the lamella surface, as noted by recent MonteCarlo simulations. The study of the melting process evidences that the degree of hysteresis is small.

PACS numbers: 61.25.Hq,02.70.Ns

Keywords: folding process, energy landscape, polymer crystals, molecular-dynamics simulations

*Electronic address: `dino.leporini@df.unipi.it`

I. INTRODUCTION

Folded states of chain-like macromolecules including proteins [1] and crystalline polymers [2–9] are under current intense study. **In spite of the large differences between homopolymers and proteins, interesting correspondences between the structural transitions of** *isolated, single homopolymer chains* **and the protein folding have been noted by both numerical simulations [10, 11] and experiments [12, 13]** . One key issue is if the morphologies of folded states are thermodynamically or kinetically controlled. In proteins the thermodynamic viewpoint is strongly supported by early studies by Pauling [14] and Anfinsen [15], while the so-called Levinthal's paradox [16] suggests that folding is kinetically controlled. Kinetic factors are believed to set the growth rate of polymer crystals [3, 5] as well as the thickening of folded macromolecules [17, 18]. While this is a safe conclusion for long chains (polymers), where large entropic barriers hamper the conformation changes leading to structures which are e.g. partially crystalline, it may be questioned for shorter chains (oligomers) which are less impeded. Relevant to the better understanding of the crystallization of chain molecules is also the observation of the transient phases that convert them to more stable forms during the folding process of n-alkanes [19] as well as the identification of metastable intermediates in the formation and melting of polymer globules in solution [12, 13]. This behaviour may be seen as a manifestation of the Ostwald step rule stating that in the course of transformation of an unstable (or metastable) state into a stable one the system does not go directly to the most stable conformation but prefers to reach intermediate stages having the closest free-energy to the initial state [20].

The crystalline state of polymers is very different from that of other materials because of the need to arrange in an ordered way a large number of monomers linked to each other sequentially. This results in a wide range of possible hierarchical morphologies where the basic unit is the lamella, which is a few hundred Ångstrom thick [3, 5–9]. The backbone of a single polymer chain, which is several thousand Ångstrom long, is folded inside the lamella to form the so-called stems; these are perpendicular to the basal surfaces of the lamella where the foldings are localized [5–7]. Different regimes in polymer crystallization are known. If impurities or seed nuclei are absent, the *primary crystallization* starts with the *primary homogeneous nucleation* of a critical-size nucleus and is followed by **a growing stage where additional chains add to the nucleus [5]** . This leads to lamellar-shaped

crystals in dilute solutions [2, 3]. If the crystallization takes place in the melt, the lamellae arrange themeself in supramolecular structures named spherulites. The mutual impingement of the spherulites sets the late stage of the crystallization which is referred to as *secondary crystallization*. Kinetic aspects of the secondary nucleation and crystallization regimes of polymers are well documented by experiments [2, 3] , theory [5] and simulations [21–25], and are understood in terms of the severe constraints exerted on the growth process by the interaction between the entangled chains and, additionally, between the impinging supramolecular structures. For oligomers, once-folded or extended conformations of the chain are observed in the crystallized melts of relatively long monodisperse n- alkanes (C_nH_{2n+2}, $150 \leq n \lesssim 390$) while up to four foldings per chain were observed in dilute solutions [4, 17, 26, 27]. The number of foldings increases with supercooling. It is believed that for *multi-chain* crystallites the extended conformation of the single chain corresponds to the global minimum of the free-energy, which may be reached from the original kinetically-selected minimum via a series of transitions through less and less folded conformations (each corresponding to different local minima) if the involved free-energy barriers can be overcome [17]. Transitions are evidenced by heating solution-grown crystals ($n = 168, 240$ [17, 18]) or melts ($n = 198, 246$ [26]) . Furthermore, aging behavior yielding transitions from folded to extended states were observed in the melt of n- alkanes by prolonged isothermal crystallization at small supercoolings ($198 \leq n \leq 390$ [4, 26]). The primary nucleation of polymers and oligomers has been investigated in the melt both by experiments [26, 28] and simulations [29]. Nonetheless, very few groups have challenged the rather problematic and related issue of the preparation of single-molecule single crystals [30, 31]. Understanding if the primary nucleation is kinetically or thermodinamically controlled is nontrivial. The difficult characterization of the primary nucleation regime in dilute solutions motivated several simulations [21–23, 32–39]. For relatively short chains, the primary nucleation of single-molecule n-alkanes with a number of monomers $N = n \leq 300$ were found to end up in the global minimum of the free-energy , i.e. in thermodynamic equilibrium, at a quench depth $\Delta T \equiv T_m - T \sim 0.2\ T_m$, where T_m is the melting temperature [21, 22]. However, the eventual kinetic arrest of the nucleation in one state during the primary nucleation of longer single-molecules cannot be excluded due to the increasing number of entanglements and, consequently, larger energy barriers.

The above discussion makes it clear that the polymer crystallization is a realistic process

to test the possibility of a thermodynamical description of out-of-equilibrium states, which is under current development in supercooled liquids, spin glasses, and biomaterials [40–50]. The fine-grained description considers the potential energy landscape (PEL), i.e. the $3N$ dimensional surface describing the dependence of the potential energy on the configurations of a system with N particles [40, 46]. Alternatively, the coarse-grained description provided by the free-energy landscape (FEL) has been considered for glasses [46–48] the dynamics and the geometry of protein folding [46, 49], the polymer crystallization [21, 22, 51], clusters [46], the melting of the subsequent cystalline nucleus [38, 39, 52] as well as other disorder-to-order transitions in isolated homopolymers [53]. Implicit in the adoption of FEL is the identification of suitable observables, the so-called order parameters, characterizing the macrostate of the physical system. FEL is a low-dimensional surface compared to the high-dimensional PEL and is obtained by averaging over all the degrees of freedom for fixed values of the order parameters [46]. At constant volume, differently from PEL, FEL is temperature-dependent with an expected richness of minima corresponding to different packings [47].

The present paper reports on a simulation, carried out by Molecular-Dynamics (MD) algorithms, of the primary nucleation of single-molecule n-alkanes with $N = 500$. Similar lengths are characteristic of polyethylene (PE) ($N \gtrsim 200$) more than paraffine waxes ($17 \lesssim N \lesssim 40$) [54]. The goal is to understand if the final state is reached by favourable kinetic paths or is set by the thermodynamics. To this aim the chain length is increased with respect to previous studies [22] to favour the onset of entanglements and then the presence of sufficiently high free-energy barriers. Nonetheless, in the range $\Delta T \leq 2$ (in reduced units) it was found that the chain reaches the global minimum of the FEL, i.e it restores the equilibrium. The global minimum is reached even if one prepares the chain in the fully stretched (all-trans) conformation and then anneals it is at the lowest temperature under investigation. Special emphasis is given to the microscopic characterization of the equilibrium state. The melting process was also investigated and compared to recent MonteCarlo studies evidencing the large supercooling and superheating of long chains [38, 39]. The paper is organized as follows. In Sec.II the PE model is outlined. In Sec. III the results are presented and discussed. The conclusions are summarized in Sec.IV.

II. NUMERICAL METHODS

The behaviour of a single PE chain with $N = 500$ monomers in solution has been studied by means of a united-atom model. The solvent is mimicked by suitable friction and random forces acting on the monomers. The chain is described as a sequence of beads, where each bead represents a single methylene CH_2 group. No distinction is made between internal methylene CH_2 groups and terminal methyl CH_3 groups in order to obtain a slight improvement in efficiency [23]. For long chains this approximation is fair. The local interactions shaping the chain are defined by the potentials

$$U_{\rm bond}(r) = k_r(r - r_0)^2 \tag{1}$$

$$U_{\rm angle}(\theta) = k_\theta(\cos\theta - \cos\theta_0)^2 \tag{2}$$

$$U_{\rm torsion}(\phi) = k_1(1 - \cos\phi) + k_2(1 - \cos 2\phi) + k_3(1 - \cos 3\phi) \tag{3}$$

$U_{\rm bond}(r)$ is a harmonic spring potential defined for every couple of adjacent beads, r being their distance and r_0 the equilibrium bond lenght. $U_{\rm angle}(\theta)$ is defined for every triplet of adjacent beads, θ being the angle between the corresponding bonds and θ_0 its equilibrium value. Finally, $U_{\rm torsion}(\phi)$ is defined for every quadruplet of adjacent beads and ϕ is the dihedral angle beween the planes defined by the corresponding three adjacent bonds. Pairs of beads not interacting by any of the preceding potentials interact by means of a Lennard-Jones potential

$$U_{\rm LJ}(r) = 4\epsilon\left[\left(\frac{\sigma}{r}\right)^{12} - \left(\frac{\sigma}{r}\right)^{6}\right] \tag{4}$$

with a cutoff radius $r_{\rm cut} = 2.5\sigma$. The set of parameters of the above force field are taken from ref. [55] (see table I). The force field enforces the local stiffness of the chain yielding a Kuhn segment length $\ell_{\rm k} \cong 1.2$ [2, 3], corresponding to segments with about four beads. Therefore, the polymer is sketched as a succession of about $N_{\rm k} = 125$ rigid segments. The corresponding time and temperature units are given by $t^* = 2.21$ ps and $T^* = 56.3$ K. All the results will be presented in terms of reduced units. For the set of parameters listed in table I the single-molecule crystal melts at $T_m = 11 \pm 0.2$ in the limit of vanishing heating rate [22, 55]. **This value is exceedingly high and calls for refinements of the force field. However, since we are interested in studies carried out by the same**

force field [21–23, 55], these adjustments are beyond the present purposes. By the way, similar problems were also noted in other studies on PE single-chain crystals which exhibited global orientational order already at $550K$ by using the DREIDING potential [34].

The dynamics is described by the Langevin equation

$$\ddot{\mathbf{r}}_i = -\nabla_i U - \Gamma \dot{\mathbf{r}}_i - \mathbf{W}_i \tag{5}$$

where $\mathbf{r}_i$ denotes the position vector of the i-th bead, $\nabla_i U$ is the sum the internal forces acting on it, $\Gamma \dot{\mathbf{r}}_i$ is the frictional force and $\mathbf{W}_i$ is a gaussian noise:

$$\langle \mathbf{W}_i(t) \cdot \mathbf{W}_j(t') \rangle = 6\Gamma k T \delta_{ij} \delta(t - t') \tag{6}$$

The friction and the random forces account for the solvent and set the temperature via the proper fluctuation-dissipation theorem. Eq.5 is integrated by means of the velocity Verlet algorithm with time step $\Delta t = 0.001$ [56, 57].

The runs are performed according to the following protocol: seventeen random chain conformations are initially equilibrated at $T_{eq} = 15$ for at least ten times the time needed for the self correlation function of the end-to-end vector to vanish. The equilibrated chain does not exhibit any local orientational order (see Sec.III A for details). The final temperature T_f is reached via different thermal histories: i) instantaneous direct quenches $T_{eq} \rightarrow T_f$, ii) instantaneous quenches with intermediate annealing at T_{ann}, $T_{eq} \rightarrow T_{ann} \rightarrow T_f$. Annealing times were 3×10^4 at $T_{ann} = 9$, 10 and 6×10^4 at $T_{ann} = 11$. The overall scheme of the thermal paths is summarized in Fig. 1. The total number of direct quenches (17) and quenches with intermediate annealing leading to one specific T_f was 28. Memory effects were also investigated by preparing a sample in the "all-trans" fully-extended conformation and isothermally annealing it at $T = 9$. Having reached T_f, data were collected during evolution times of 3×10^4 at $T = 9$, 10 and 6×10^4 at $T = 11$. The all-trans conformation was monitored after the initial preparation for 3×10^4 time units.

In order to evaluate the Landau free energy $F(X) = -kT ln\ Z(T, X)$ of a macroscopic state being characterized by the order parameter X at temperature T leading to a partition function $Z(T, X)$, one relates the latter to the probability $P(X)$ to find the observable with value X via [58]

$$P(T,X) = Z(T,X)/Z(T) \tag{7}$$

and $Z(T)$ is the partition function. Then, up to an additive constant $c(T)$ depending on the temperature $F(X)$ is given by [38, 39, 59]

$$F(X) = -kT\, ln\ P(T,X) + c(T) \tag{8}$$

Since only the shape of $F(X)$ is of interest here, the constant $c(T)$ will be neglected henceforth.

III. RESULTS AND DISCUSSION

Results on the crystallization process after quenches below the melting temperature $T_m = 11 \pm 0.2$ are first presented in Sec. III A. The long-time properties of the chains at different quench depths $\Delta T = T_m - T$ are characterized in Sec. III B and Sec.III C. The chain melting is discussed in Sec. III D.

A. The crystallization process

1. Kinetics

The kinetics of the crystallization process is nontrivial and depends on the chain conformation. Fig. 2 shows some representative snapshots evidencing that the chain gathers relatively long straight sections (the so-called stems) to form the overall ordered structure. The nucleation may involve either the whole chain or separate portions merging at later times by reeling in their connector. The latter process has been already noted for much longer chains ($N = 2000$)[22, 55]. Fig. 2 shows that it also occurs in shorter chains.

In principle, owing to the different scenarios of the nucleation, the kinetic arrest in different states cannot be ruled out . Tracking the amount of alignment between different sections of the chain by means of suitable order parameters is of help in order to assess that hypothesis. To this aim, one defines

$$\mathbf{b}_i = \frac{\mathbf{r}_{i+1} - \mathbf{r}_{i-1}}{|\mathbf{r}_{i+1} - \mathbf{r}_{i-1}|} \tag{9}$$

$\mathbf{b}_i$ is thus a unit vector locally aligned with the chain backbone. The order parameter is defined as [23]

$$S = \langle P_2(\mathbf{b}_i \cdot \mathbf{b}_j)\rangle_{i>j} \tag{10}$$

where $P_2(x)$ denotes the second Legendre polynomial in the variable x and the average is computed for all the pairs of inner monomers . Fully disordered and ordered states yield $S = 0$ and $S = 1$, respectively.

Fig. 3 (top) shows the time evolution of the order parameter S of the chain for all the investigated thermal histories leading to $T_f = 9$. Direct quenches from $T_{eq} = 15$ and quenches after the annealing at $T_{ann} = 10$ exhibit at short times ($t \lesssim 5$) the pre-quench order parameters $\langle S\rangle_{T_{eq}} = (1.31\pm0.03)\times10^{-2}$, $\langle S\rangle_{T_{ann}} = (3.4\pm0.18)\times10^{-1}$, respectively. For the all-trans initial conformation S drops from the unit value. Note that the spread of the curves is much larger at intermediate times than immediately after the quench evidencing that the crystallization paths may be somewhat different from each other [60]. Nonetheless, at long times the paths become closer and , after a transient period of about 2×10^4 time units, indipendently of the thermal history, the chain exhibits the order parameter $\langle S\rangle_{T=9} = (5.10\pm0.18)\times10^{-1}$, i.e. at long times the time average of a single history coincides within the errors with the ensemble average over all the different histories. Henceforth, the chain conformations at $T_f = 9$ after the transient period will be referred to as belonging to the crystalline *final state* . Fig. 4 shows one conformation of the final state. It is a well-defined lamella with two small-sized caps where the loops connecting the stems are localized. The stems have approximately equal length. In Sec.III B it will be seen that they are arranged into a regular, hexagonal pattern and their number μ is well defined ($\mu = 10$), i.e. the general features of the final state are largely independent of the thermal history. In fact, Fig. 3 shows that the order-parameter distributions P_S for the final states of all the thermal histories are quite similar within the statistical errors. P_S peaks at $S \sim 0.52$ evidencing considerable chain order. The distribution is skewed to the low S-values. This is ascribed to the disorder localized in the two crystal caps as well as in the crystal surface (see Sec. III B).

To characterize the different kinetic pathways leading to the final crystal state the inertia tensor of the conformations was considered. The principal axes $\{1, 2, 3\}$ are ordered according to the magnitude of the corresponding eigenvalue which are labelled as I_1, I_2 and I_3, I_1 being the largest one. Fig.5 (top panel

) plots the time -dependence of I_1 of both selected quenches at $T = 9$ and the isothermal annealing of the initially fully-extended conformation at the same temperature. The plot gives insight into the typical structural changes leading to the final crystal state. It is seen that the changes occur as fast transitions in about few hundreds of time units between states with different, discrete I_1 values. Such states are identified by visual inspection as ordered conformations with different number of stems. At long times all the pathways converge to a single state with $I_1 \cong 10^4$, i.e. the final state with a number of stems $\mu = 10$. The time -dependence of I_1 evidences transitions with changes of the number of stems $\Delta\mu = \pm 1, -2$ and even a quasi-transition with $\Delta\mu = -4$, i.e. two transitions with $\Delta\mu = -2$ being very close to each other. Transitions with $\Delta\mu = \pm 1$ involve stems terminated by one of the two chain ends. Transitions with $\Delta\mu = -2$ involve stems built by inner portions of the chain. Transitions with $\Delta\mu = +2$ were not observed. Notice that the approach to the final state ($\mu = 10$) is not monotonous, e.g. in Fig.5 a transition is seen from one state with $\mu = 11$ to one with $\mu = 9$. Fig.5 (middle panel) shows selected snapshots of one transition with $\Delta\mu = -1$ involving a chain end (transitions with $\Delta\mu = +1$ are quite analogous to the same sequence in reverse time order). Fig.5 (bottom panel) shows selected snapshots of one transition with $\Delta\mu = -2$. It is interesting to note that the stems disappearing (or being created) during the transitions are always seen to be located on the crystal surface.

2. Free-energy landscape

Fig. 6 shows the free-energy landscape (FEL) at $T = 9, 10, 11$ as a function of the largest moment of inertia of the chain I_1. At $T = 11$ a single minimum is observed at $I_1 = I_1^* \sim 4900$. Later, it will be shown that at that temperature the chain is spending most time as a random coil (see Sec. III D). On decreasing the temperature and entering the supercooled regime at $T = 10$ the minimum at I_1^* disappears and a series of shallow minima is observed at higher I_1 values ($I_1 \gtrsim 5500$) . They correspond to the formation of metastable crystal structures with different number of stems μ (see Sec. III C). The direct inspection of the dynamical behaviour of the chain at $T = 10$ shows that a continuous

interconversion between the metastable structures occurs with no well-defined single final state. At $T = 9$ the FEL exhibits a richer structure with several minima. A well-defined global minimum is apparent corresponding to the final state with $\mu = 10$ (see Sec. III B). It is also seen that lowering the temperature allows the appearance of new metastable ordered states which, as at $T = 10$, may be labeled by the number of stems. The comparison with the FEL of shorter chains at $T = 9$ [21, 22] shows that the number of metastable states increases with the chain length. The presence of metastable and long-lived crystalline forms is supported by a number of experimental facts, e.g. the observation of the transient phases that convert to more stable forms during the folding process [19] and the demonstration of stable folded structures for long alkanes, $N \gtrsim 150$, [3–5, 26].

B. The crystalline final state

1. Moments of inertia.

In order to get a deeper understanding of the structure of the crystallized chains, the inertia tensor of the conformations in the final state at $T = 9$ was analyzed. Fig. 7 plots the distributions of the three eigenvalues I_1, I_2 and I_3 for all the thermal histories. The average values over all the thermal hystories are $\langle I_1 \rangle = 10097 \pm 58$, $\langle I_2 \rangle = 9885 \pm 51$, $\langle I_3 \rangle = 1148 \pm 11$. Since $\langle I_1 \rangle \gtrsim \langle I_2 \rangle \gg \langle I_3 \rangle$, the ellipsoid of inertia of the crystal exhibits approximate cylindrical symmetry around the **3** axis, as it may be seen by visual inspection (see Figs. 2, 4). Fig. 7 shows that the shape of the distributions for the largest eigenvalues P_1 and P_2 is nearly symmetric with small width whereas the distribution for the smallest eigenvalue P_3 is rather asymmetric, larger and skewed to higher I_3 values. The skewness must be ascribed to the structural changes occurring on the crystal surface (see below).

2. Longitudinal monomer distribution: small caps

In order to analyze the crystal structure one defines the monomer distribution function $\rho(\mathbf{r})$ as

$$\rho(\mathbf{r}) = \frac{1}{N} \sum_{i=1}^{N} \left\langle \delta(\mathbf{r} - \mathbf{r}_i^{(\mathrm{cm})}) \right\rangle \tag{11}$$

where $\mathbf{r}_i^{(\mathrm{cm})}$ is the position of the i-th bead with respect to the center of mass of the chain and the brackets denote a suitable average. In particular, one defines the quantity

$$N_{||}(x^3) = N\,d \times \int \rho(x^1, x^2, x^3)\, dx^1 dx^2 \tag{12}$$

where $d \equiv r_0 \sin\left(\frac{\theta_0}{2}\right) \simeq 0.31$ is the distance along the chain backbone between two adjacent beads of the fully-extended chain and x^k is the projection of $\mathbf{r}$ along the $k-$th principal axis. The quantity $N_{||}(z)$ denotes the number of intersections of the chain with the plane at $x^3 = z$, namely a plan perpendicular to the approximate cylindrical symmetry x^3 axis. Fig. 8 plots the quantity $N_{||}(z)$ in the final crystalline state at $T = 9$ for all the thermal histories. It is apparent that the dependence of $N_{||}(z)$ on the thermal history is negligible. A fortiori, this holds true for the number of stems $\mu = N_{||}(0) = 10$, corresponding to the conformation yielding the global minimum of the free-energy (fig. 6). Three different regions are seen in Fig. 8:

- the central region, $|z| \lesssim L_{\mathrm{c}}/2$ with $L_{\mathrm{c}} = 8$, where $N_{||} \simeq 10$;
- the transition region, $L_{\mathrm{c}}/2 \lesssim |z| \lesssim L_{\mathrm{c}}/2+2$ where the average orientation of the stems departs from the one of the x^3 axis;
- the end region, $|z| \gtrsim L_{\mathrm{c}}/2 + 2$, where the stems join each other by forming loops.

Fig. 8 shows that the shape of $N_{||}(z)$ is very close to the ideal one corresponding to ten parallel, all-trans stems of fifty monomers each. The comparison makes it more apparent both the order in the final state and the small size of the two crystal caps. In fact, the longitudinal size of the loops, $\Delta z \sim 3$, is fairly smaller than the crystal length $2L_{\mathrm{c}} = 16$. Notice that, since $I_3 \ll I_\perp$ with $I_\perp = (I_1 + I_2)/2 \simeq 9990$, the folded chain may be sketched as a rigid rod with lenght $2L$, mass N and negligible thickness. The approximation yields $L = \sqrt{3I_\perp/N} \simeq 7.74$, to be compared with $L_{\mathrm{c}} \sim 8$, as drawn from Fig. 8.

Both previous experimental [4] and numerical [36] works pointed out the sharpness of the loops connecting the different stems and motivated a recent model of the FEL global minimum of the single-molecule polymer crystals [37].

3. Transverse monomer distribution: surface mobility

In order to study the monomer distribution in planes perpendicular to the x_3 axis one defines

$$\rho_{\perp,\mathrm{centr}}(\mathbf{x}_\perp) = \int_{-L_c/2}^{L_c/2} \rho(\mathbf{x}_\perp, z)\, dz \tag{13}$$

$$\rho_{\perp,\mathrm{trans}}(\mathbf{x}_\perp) = \int_{L_c/2}^{L_c/2+2} [\rho(\mathbf{x}_\perp, z) + \rho(\mathbf{x}_\perp, -z)]\, dz \tag{14}$$

$$\rho_{\perp,\mathrm{term}}(\mathbf{x}_\perp) = \int_{L_c/2+2}^{\infty} [\rho(\mathbf{x}_\perp, z) + \rho(\mathbf{x}_\perp, -z)]\, dz \tag{15}$$

where $\mathbf{x}_\perp = x^1\mathbf{1} + x^2\mathbf{2}$ denotes the position vector in the transverse plane. $\rho_{\perp,\mathrm{centr}}(\mathbf{x}_\perp)$, $\rho_{\perp,\mathrm{trans}}(\mathbf{x}_\perp)$ and $\rho_{\perp,\mathrm{term}}(\mathbf{x}_\perp)$ are the transverse monomer distributions in the central, transition and end regions, respectively. Fig. 9 shows the tomography of the crystal structure. First, the crystal structure achieved after one particular thermal history (left panels) is compared with the average of all the investigated thermal histories (right panels). Data are collected during a lapse of time of about 5×10^3 time units. The absence of any significant difference is apparent and proves once again the absence of any memory effect, namely that at $T = 9$ the final crystalline state corresponds to the global minimum of the free-energy which is seen in Fig. 6. The tomography evidences several features of the crystal structure. The ten stems of the crystalline nucleus arrange themselves into an hexagonal structure (top plots). Noticeably, there is virtually no order on the crystal surface. Moving to the caps of the crystal structure the amount of order decreases. The transition region (center plots) still retains a partially ordered structure, visible in the two central stems, whereas the remaining eight external stems become more mobile. In the end regions (bottom plots), where the loops connecting the stems are located, any ordered structure is lost. It must be pointed out that the absence of order on the crystal surface and the two caps is due to the mobility of the chain in that regions, as it may be appreciated in the left plots of Fig. 9, which monitor the monomer transverse distribution for a single chain over a finite time interval. The presence of a disordered "corona" surrounding the ordered fraction of the nucleus has been noted by MonteCarlo simulations [38]. In the present case the direct inspection of several snapshots shows that the crystal surface is highly mobile and includes the chain ends which are excluded from the crystal interior. The confinement of the end

groups on the surface avoids the impairment of lattice perfection and agrees with previous experimental findings [4].

It is worthwhile to appreciate the role of the mobile fraction of monomers of the crystalline final structure at $T = 9$. In thermodynamic equilibrium, fixed-volume systems minimize the Helmholtz free-energy F. Correspondingly, the state point moves between several potential-energy minima (the mechanical equilibrium states) in a region of PEL determined by the temperature. When the temperature decreases, the state point spends more time in the deeper, rarer minima of PEL. If crystallization occurs, the state point becomes localized in the global minimum of PEL. The global minimum is usually not degenerate and the shape of the corresponding minimum of F stems from vibrational dynamics providing suitable contributions to both the internal energy and the entropy. In the present case the region of PEL where the state point localizes at $T = 9$ is highly degenerate due to the different surface configurations of the crystallized chain. Thus, the configurational contributions to F are not negligible even in the crystalline state.

The results discussed in the present Section allow one to conclude that in the final crystalline state at $T = 9$ the chain packs into ten stems, of approximately equal lenght, arranged into a regular pattern with hexagonal symmetry. The ordered structure cannot include all the beads because of the chain connectivity and of the local potentials, which e.g. generically do not allow a regular packing of chain bendings. The disorder is expelled into the two caps and on the surface, where the structural fluctuations take place. Remarkably, the end regions where the loops connecting the stems are located have small size (see figs. 4 and 8).

C. The crystalline metastable states

Fig. 2 presents some representative snapshots showing that the chain, after the quench at $T = 9$, undergoes large conformation changes in order to reach the crystalline final state. The FEL structure at $T = 9$, Fig. 6, elucidates the state evolution starting at some point characterized by a certain I_1 value, going through a number of transient ordered phases with well-defined number of stems, and ending in the global minimum. n- alkanes are known to have intermediate metastable forms on the path to the final crystalline state [19].

For the different metastable crystalline states at $T = 9$, evidenced by the minima of FEL (Fig. 6), Fig. 10 shows the number of intersections of the chain $N_{||}(z)$ with the plane

at $x^3 = z$, perpendicular to the approximate cylindrical symmetry x^3 axis. The flatness of $N_{||}(z)$ shows that the central sections of the metastable structure are well ordered. It is also apparent that the monomer distribution in the end sections does not depend in a marked way on the number of stems $\mu = N_{||}(0)$. To be more quantitative, we consider the crystalline fraction ϕ_{cry} of a crystal with μ stems. ϕ_{cry} is estimated by the ratio

$$\phi_{cry} = \frac{\int_{z^1_{max}}^{z^2_{max}} N_{||}(z)dz}{\int_{-\infty}^{\infty} N_{||}(z)dz} \tag{16}$$

where z^1_{max} and z^2_{max} are the points where $N_{||}(z)$ reaches the maximum values, see Fig. 10. **Obviously, the amount of crystalline order in a single-molecule crystal may be defined in alternative ways, e.g. in terms of bunches of orientationally ordered trans segments, "trans domains" [34]. However, we found that the definition eq.16 is quite fruitful to our purposes. In fact,** let us assume that an average number of Kuhn segments λ is located in each of the $\mu - 1$ loops connecting the stems. Then, the crystalline fraction is given by

$$\phi_{cry} = 1 - (\mu - 1)\frac{\lambda}{N_k}. \tag{17}$$

The inset of Fig. 10 shows the best-fit of ϕ_{cry} from eq.16 with eq.17 having adjusted λ. It proves that the number of monomers forming the loops do not change appreciably from one transient structure to the other. At the highest number of stems (shortest crystal longitudinal size) eq.17 overestimates ϕ_{cry} suggesting that the disorder of the end sections affects the ordered part more effectively (or, alternatively, that λ increases).

As further test of the negligible changes of λ with μ we note that the number of Kuhn segments per stem m is expressed as $m = (z^2_{max} - z^1_{max})/\ell_{\rm k}$. On the other hand, if λ is nearly constant

$$m^* = \frac{N_k - \lambda\,(\mu - 1)}{\mu} \tag{18}$$

Table II compares m with m^* as taken from Eq.18 with $\lambda = 4$.

D. Melting

The equilibrium melting temperature $T_m^{(eq)}$ is, by definition [39], the temperature where the free-energies of the ordered and the disordered states are equal. An estimate is given by melting the crystal in the limit of vanishing heating rates. By following that method the single-molecule crystal was found to melt at $T_m = 11 \pm 0.2$ for the force-field in use [22, 55].

The FEL (fig. 6) shows that $10 < T_m^{(eq)} < 11$ since the ordered states ($I_1 \gtrsim 5500$) have higher (lower) F values at $T = 11$ ($T = 10$) than the disordered one ($I_1 \sim 5000$). Noticeably, at $T = 10$ the crystal is not stable but it undergoes frequent interconversions between different ordered structures as signaled by the shallow minima of the FEL and visual inspection of the snapshots (data not shown).

Both the single minimum of F corresponding to the disordered state at $T = 11$ and the small barrier heights at $T = 10$ suggest the negligible superheating of the crystal. To clarify the point, $T = 11$ was reached by: i) instantaneously quenching three equilibrated configurations at $T = 15$ and ii) instantaneously heating three configurations of the crystalline final state at $T = 9$. Fig. 11 shows the subsequent temporal changes of the order parameter S. After the sudden heating, the melting of the crystal is signaled by the large drop in the order parameter S and exhibits large fluctuations at long times. Similar fluctuations are also observed for the quenched configurations. The inspection of several snapshots suggests that the long-time behaviour at $T = 11$ is independent of the thermal history. Fig. 11 shows the fluctuations of the order parameter for one selected thermal history at long times and the corresponding chain conformations. It is seen that the large fluctuations are due to infrequent attempts to crystallize of the chain. This behaviour, leading to large energy fluctuations (not shown), is a consequence of the proximity of $T_m^{(eq)}$ to $T = 11$ [38, 39]. The FEL at $T = 11$ shows that thermal fluctuations of about $3kT$ are needed for ordering the structure, i.e. for increasing I_1 from about $5 \cdot 10^3$ to about 10^4. To characterize the process, the waiting-time distribution $\psi(t)$ between two successive crystallization attempts was evaluated. An attempt is defined as an event with *average* order parameter $\bar{S} > S_{\text{treshold}} = 0.12$ over 50 time units. The waiting-time distribution is found to be roughly exponential (Fig. 12), suggesting that the attempts are independent events.

The results discussed in this section provide upper limits for the degree of superheating/supercooling of the present PE model. One defines $\varepsilon = (T_m^* - T_f^*)/T_f^* \geq 0$, T_m^* and T_f^*

being the melting temperature on heating and the freezing temperature on cooling, respectively. Being $10 < T_m^*, T_f^* < 11$, it is found $\varepsilon < 0.1$. i.e. small hysteresis.

The melting of crystalline polymers has been recently studied by MonteCarlo simulations [38, 39, 52]. In particular, the superheating of the single crystals, as well as the supercooling of the disordered state, have been noted for single chains with a number of monomers $N \gtrsim 100$ resulting in large hysteresis and dependence on the thermal history [38, 39]. To proceed with a comparison with the present results some remarks must be done. The MonteCarlo simulations sketch the polymer as a fully flexible linear chain of N rigid segments [38, 39]. It is natural to identify that segments with the Kuhn segments. As noted in Sec.II) the number of Kuhn segment of the present PE model is about $N_{\rm k} = 125$. For $N \cong 125$ the results of refs. [38, 39] yield $\varepsilon \cong 0.1$ in good agreement with the present ones.

IV. CONCLUSIONS

The paper presented numerical results from extensive MD simulations of the crystallization process of a single PE chain with $N = 500$ monomers. The chain, after suitable equilibration at high temperature is cooled at the final temperature T_f by quenches involving or not intermediate annealing steps at T_{ann}. In addition, it is also isothermally annealed at T_f after initial preparation in the fully-stretched "all-trans" configuration. At $T_f = 11$ the chain remains amorphous for most time with occasional attempts to crystallize. For $T_f < 11$ the development of the ordered structure proceeds along different routes involving either the global reorganization of the chain or, alternatively, well-separated connected nuclei. The latter process was previously observed only for much longer chains. Differently from the early crystallization stages, no dependence on the thermal history was observed at late stages. At $T_f = 10$ the chain does not reach a single stationary state but continuously converts between different ordered configurations to be described elsewhere [60]. At $T_f = 9$ the folding process of the chain involves several intermediate ordered metastable states in strong analogy with the experiments on n-alkanes [19] which finally yields a well-defined long-lived lamella with ten stems of approximately equal lenght, arranged into a regular, hexagonal pattern. We take the evidence of metastable intermediate states as a *microscopic* manifestation of the Ostwald step rule stating that in the course of transformation of an unstable (or metastable) state into a stable one the system does not go directly to the most

stable conformation but prefers to reach intermediate stages having the closest free-energy to the initial state [20]. Both the metastable states and the long-lived one are well evidenced as local and global minima of the free-energy landscape (FEL), respectively.

The characterization of the microscopic organization of the lamella evidenced that the two caps are rather flat, i.e. the loops connecting the stems are short, a conclusions which may be also drawn from other experimental [4] and numerical studies [36]. Interestingly, annealing the chain through the different metastable states leaves the average number of Kuhn segments per loop λ nearly unchanged. It is also seen that the chain ends, the so-called cilia, are localized on the surface of the lamella, in agreement with the experiments [4], and that structural fluctuations take place on the lamella surface, as noted by recent MonteCarlo simulations [38]. This shows that the global minimum of FEL corresponds to a set of microscopic states with the same crystalline core and different surface configurations of the cilia and the two caps. The findings will be of help to improve a recent analytic model of the global minimum of the FEL [37].

Finally, the study of the melting process evidenced that the degree of hysteresis is small, in agreement with other MonteCarlo studies. Furthermore, at temperatures a little bit higher than the freezing one, independent attempts to crystallize the chain has been observed.

V. ACKNOWLEDGEMENTS

The careful reading of the manuscript by A.Barbieri is warmly thanked. Financial support from MIUR within the PRIN project "Dynamics and Thermodynamics in out-of-equilibrium materials: structural glasses, gels, polymeric materials" is gratefully acknowledged.

---

[1] M.Gruebele, Ann.Rev.Phys.Chem. **50**, 485 (1999).

[2] U. W.Gedde, *Polymer Physics* (Chapman and Hall, London, 1995).

[3] G. Strobl, *The Physics of Polymers* (Springer, New York, 1997).

[4] G. Ungar, J. Stejny, A. Keller, I. Bidd, M.C. Whiting, Science **229**, 386 (1985).

[5] K. Armitstead, G. Goldbeck-Wood, Adv. Polym. Sci. **100**, 219 (1992).

[6] A. Keller, Rep. Prog. Phys. **31**, 623 (1968).

[7] P.J. Philips, Rep. Prog. Phys. **53**, 549 (1990).

[8] G. Strobl, Eur. Phys. J. E **3**, 165 (2000).

[9] M. Muthukumar, Eur. Phys. J. E **3**, 195 (2000).

[10] Y.Zhou, C.K.Hall, M.Karplus, Phys.Rev.Lett. **77**, 2822 (1996).

[11] Y.Zhou, M.Karplus, J.M.Wichert, C.K.Hall, J. Chem. Phys. **107**, 10691 (1997).

[12] C.Wu, S.Zhou, Phys.Rev.Lett. **77**, 3053 (1996).

[13] C.Wu, S.Zhou, Macromolecules **28**, 8381 (1995).

[14] A.E.Mirsky, L.Pauling, Proc.Natl.Acad.Sci. USA **22**, 439 (1936).

[15] C.B.Anfinsen, E.Haber, M.Sela, F.White Jr., Proc.Natl.Acad.Sci. USA **47**, 1309 (1961).

[16] C.Levinthal in *Mossbauer Spectroscopy in Biological Systems*, P.Debrunner, J.C.M Tsibris, E. Münck edts. (University of Illinois Press, Urbana, 1969).

[17] G. Alamo, L. Mandelkern, G.M. Stack, C. Krohnke, G. Wegner, Macromolecules **26**, 2743 (1993).

[18] G. Alamo, L. Mandelkern, G.M. Stack, C. Krohnke, G. Wegner, Macromolecules **27**, 147 (1994).

[19] E.B.Sirota, A.B.Herhold, Science **283**, 529 (1999).

[20] W. Ostwald, Z. Phys. Chem. **22**, 289 (1897).

[21] P. Welch, M. Muthukumar, Phys. Rev. Lett. **87**, 218302 (2001).

[22] M. Muthukumar, Phil.Trans. R.Soc. Lond. A **361**, 539 (2003).

[23] C. Liu, M. Muthukumar, J. Chem. Phys. **109**, 2536 (1998).

[24] J.P.K.Doye , D.Frenkel, J. Chem. Phys. **110**, 7073 (1999).

[25] J.-U. Sommer, G. Reiter, Europhys. Lett. **56**, 755 (2001).

[26] S.J. Organ ,A. Keller ,M. Hikosaka ,G. Ungar, Polymer **37**, 2517 (1996).

[27] G. Ungar, A. Keller, Polymer **27**, 1835 (1986).

[28] S.K.Ghosh, M.Hikosaka, A.Toda, S.Yamazaki, K.Yamada, Macromolecules **35**, 6985 (2002).

[29] R.H. Gee , L.E. Fried, J. Chem. Phys. **118**, 3827 (2003).

[30] H. Bu, Y. Pang, D. Song, T. Yu, T. M. Voll, G. Czornyj, B. Wunderlich, J.Polymer Sci., Part B: Polym. Phys. **29**, 139 (1991).

[31] L.Z.Liu , F.Y.Su , H.S.Zhu , H.Li , E.L.Zhou , R.F.Yan , R.Y.Qian, J.Macromol.Sci.,Phys.B, **36**, 195 (1997).

[32] T.A. Kavassalis, P.R. Sundararajan, Macromolecules **26**, 4144 (1993).

[33] P.R. Sundararajan, T.A. Kavassalis,J. Chem. Soc. Faraday Trans. **91**,2541 (1995).

[34] S. Fujiwara, T. Sato, J. Chem. Phys. **114**, 6455 (2001).

[35] S. Fujiwara, T. Sato, J. Chem. Phys. **110**, 9757 (1999).

[36] H.Meyer, F. Muller-Plathe, J. Chem. Phys. **115**, 7807 (2001).

[37] L. Larini, A. Barbieri, D. Prevosto, P.A. Rolla, D. Leporini, J. Phys.: Condens. Matter **17**, L199 (2005) .

[38] W.Hu , D.Frenkel, V.B.F.Mathot, J. Chem. Phys. **118**, 3455 (2003).

[39] W.Hu , D.Frenkel, V.B.F.Mathot, Macromolecules **36**, 8178 (2003).

[40] P. G. Debenedetti, F. H. Stillinger, Nature (London) **410**, 259 (2001).

[41] C.A.Angell , Nature (London) **393**, 521 (1998).

[42] M.Mezard, G. Parisi, Phys. Rev. Lett. **82**, 747 (1999).

[43] B. Coluzzi, G.Parisi, P.Verrocchio, Phys. Rev. Lett. **84**, 306 (2000).

[44] L.-M.Martinez, C.A.Angell, Nature (London) **410**, 663 (2001).

[45] E.La Nave, S.Mossa, F. Sciortino, Phys. Rev. Lett. **88**, 225701 (2002).

[46] D.J.Wales, *Energy Landscapes* (Cambridge University Press, Cambridge, 2003).

[47] C.A.Angell, J.Res.NIST **102**, 171 (1997).

[48] L. Angelani, G. Parisi, G. Ruocco, and G. Viliani, Phys. Rev. Lett. **81**, 4648 (1998).

[49] P.G.Wolynes, J.N.Onuchic, D.Thirumalai, Science **267**, 1619 (1995); J.N.Onuchic, Z.Luthey-Schulten,P.G.Wolynes, Ann.Rev.Phys.Chem. **48**, 545 (1997).

[50] P.G.Debenedetti, *Metastable Liquids* (Princeton University Press, Princeton, 1996).

[51] J.P.K. Doye, Polymer **41**, 8857 (2000).

[52] W.Hu , J. Chem. Phys. **113**, 3901 (2000).

[53] Y.Zhou, C.K.Hall, M.Karplus, Phys. Rev. Lett. **77**, 2822 (1996); Y.Zhou, M.Karplus, J.M.Wichert, C.K.Hall, J. Chem. Phys. **107**, 10691 (1997).

[54] H.Kraack, M.Deutsch, E.B.Sirota, Macromolecules **33**, 6174 (2000).

[55] M. Muthukumar, P. Welch, Polymer **41**, 8833 (2000).

[56] M.P. Allen, D.J. Tildesley, *Computer Simulation of Liquids* (Clarendon, Oxford, 1987).

[57] D.C. Rapaport, *The Art of Molecular Dynamics Simulation* (Cambridge University Press, Cambridge, 1995).

[58] J.Lee, J.M.Kosterlitz, Phys. Rev. Lett. **65**, 137 (1990).

[59] D.Frenkel, B.Smit, *Understanding molecular simulation*, 2nd Ed. (Academic Press, New York, 2002).

[60] L.Larini, D.Leporini, work in progress.

Tables

TABLE I: Parameters of the force field.

Parameter	**Value**	
	reduced units	SI units
ϵ	1	0.112 kcal/mol
σ	1	4.04 Å
m	1	14.03 g/mol
Γ	1	0.455 Hz/mol
k_r	51005	350 kcal/mol Å^2
r_0	0.38	1.53 Å
k_θ	535.71	60 kcal/mol
θ_0	109°	109°
k_1	26.96	3.02 kcal/mol
k_2	-5	-0.56 kcal/mol
k_3	23.04	2.58 kcal/mol

TABLE II: Test of Eq.18 with $\lambda = 4$

μ	m	m^*
7	14.0	14.43
8	12.2	12.12
9	10.25	10.33
10	8.75	8.9
11	7.5	7.73
12	6.25	6.75
13	5.0	5.92

Figure captions

FIG. 1: Thermal histories leading to the final temperature T_f. Downward arrows on the left side of the figure denote the direct quenches from $T_{eq} = 15$ to T_f. Arrows on the right side denote the heating/cooling steps to reach T_f after the annealing period at T_{ann}.

FIG. 2: Wire-frame snapshots of the crystallization of a single polyethylene chain with $N = 500$ monomers for two different initial states: chain equilibrated at $T_{eq} = 15$ and quenched at $T_f = 9$ (top); chain initially in the fully-stretched configuration (all-trans) and isothermally annealed at $T = 9$ (bottom). For the latter case note the presence of initial distinct nucleation sites merging at later times.

FIG. 3: Top: time evolution of the order parameter S (eq.10) for all the investigated thermal histories leading to $T_f = 9$ (top): direct quenches from $T_{eq} = 15$ (dotted lines) and quenches after annealing at $T_{ann} = 10$ (solid lines). The thicker lines are the average order parameter for each set of curves. The dot-dashed line refers to the chain initially in the fully-stretched configuration and then annealed at $T = 9$. Bottom: order-parameter distributions P_S (dotted lines) for all the thermal histories. The solid line is the average distribution. **For a given history P_S was evaluated by counting and partitioning in a suitable histogram the conformations, each labelled by its S value, assumed by the chain for times such that $2 \times 10^4 < t < 3 \times 10^4$.**

FIG. 4: Wire-frame view of one conformation of the single-molecule crystal in the final state at $T = 9$. Note the short loops connecting the stems.

FIG. 5: **Kinetic pathways of the crystal formation. Top: Pathways of selected thermal histories leading to the final crystal state as characterized by the time dependence of the largest eigenvalue of the inertia tensor I_1. The time starts 10^2 time units after either the quench at $T = 9$ or, for the "all-trans" curve, the beginning of the isothermal annealing of the fully-extended conformation at $T = 9$. The horizontal dashed lines mark the I_1 values corresponding to crystal structures with a number of stems equal to (from the top to the bottom)** $9, 10, 11, 12, 13, 14$**. The inset is a magnification of two transitions involving the disappearance of either one (** T_1 **) or two stems (** T_2 **). Middle: Snapshots of the molecular conformations during the T1 transition occurring at times** 8200 **(A),** 8420 **(B),**8450 **(C),**8600 **(D) being marked by dots in the top panel. The cartoons below the wire-frame view sketch the rearrangements of the thick portion of the chain end involved in the transition. Bottom: Snapshots of the molecular conformations during the T2 transition occurring at times** 14800 **(E),** 14900 **(F),**15000 **(G),**15200 **(H). The cartoons below the wire-frame view sketch the rearrangements of the thick portion of the chain involved in the transition. Notice that the stems disappearing in both the T1 and T2 transitions are located on the crystal surface.**

FIG. 6: The free-energy landscape (FEL) at $T = 9, 10, 11$ as a function of the largest moment of inertia of the chain I_1. The labels indicate the number of stems μ of the ordered structures corresponding to the minima.

FIG. 7: The distributions of the moments of inertia along the transverse x^1, x^2 (top) and the longitudinal x^3 (bottom) axes in the final state at $T = 9$(see Fig. 4) . The dotted lines refer to the different thermal histories . The solid lines are the averages. **For a given history the distributions were evaluated by counting and partitioning in a suitable histogram the conformations, each labelled by the triad of moments of inertia, assumed by the chain for times such that** $2 \times 10^4 < t < 3 \times 10^4$.

FIG. 8: The number of intersections of the chain with the plane at $x^3 = z$, $N_{||}(z)$, in the final crystalline state at $T = 9$. The plane is perpendicular to the approximate cylindrical symmetry axis x^3. The different curves refer to all the thermal histories ending at $T = 9$. The dashed line is the distribution corresponding to the ideal case of ten parallel and fully extended stems with fifty monomers each. The number of stems μ is equal to $N_{||}(0) = 10$. Note the steep decrease at the end region evidencing the small size of the loops connecting the stems.

FIG. 9: Tomography of the crystal final state. The transverse distributions $\rho_{\perp,\mathrm{centr}}$ (top), $\rho_{\perp,\mathrm{trans}}$ (center) and $\rho_{\perp,\mathrm{term}}$ (bottom) (Eqs. 13-15), for one particular thermal history, i.e. a direct quench from $T = 15$, (left panels) and averaged over all the thermal histories (right panels). Note: i) the independence of the tomography on the thermal history, ii) the absence of ordered structures on the crystal surface and the two caps.

FIG. 10: The number of intersections of the chain with the plane at $x^3 = z$, $N_{||}(z)$, for the different metastable crystalline states at $T = 9$ evidenced by the minima of FEL (Fig. 6). The number of stems $\mu = N_{||}(0)$ is in the range $7 < \mu < 13$. The crystal with $\mu = 10$ stems corresponds to the final equilibrated state. Inset: The crystalline fraction ϕ_{cry} (eq.16) vs. the number of stems μ. The superimposed line is eq.17 with $\lambda = 4.0 \pm 0.1$.

FIG. 11: Top: time evolution of the order parameter S for different thermal histories ending at $T = 11$ (top); the dotted lines refer to quenches from $T = 15$, the solid lines to reheating from the crystalline final state at $T = 9$. The thick lines represent the average of the corresponding group of curves. Bottom: Fluctuations of the order parameter for one selected thermal history at long times. For some selected S values the corresponding chain conformations are shown.

FIG. 12: Waiting-time distribution of the crystallization attempts at $T = 11$ (see text for details). The solid line is a fit with an exponential decay with time constant $\tau = 805 \pm 5$.

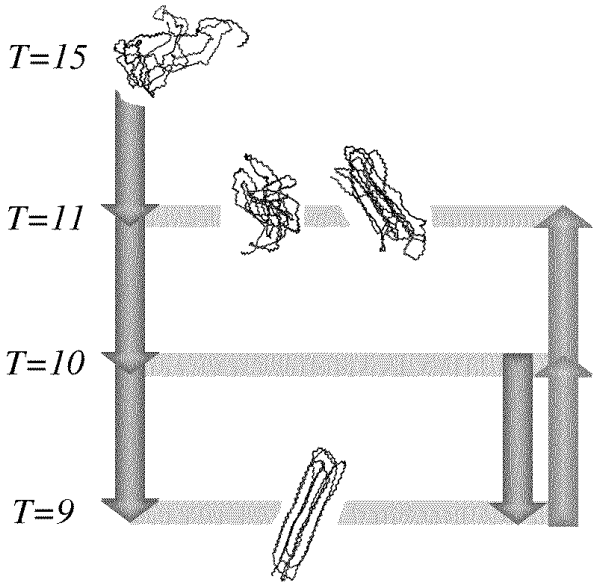

FIGURE 1

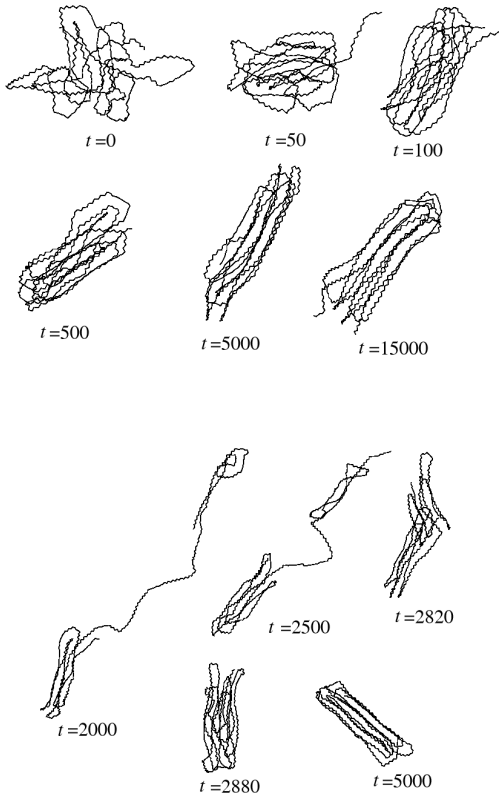

FIGURE 2

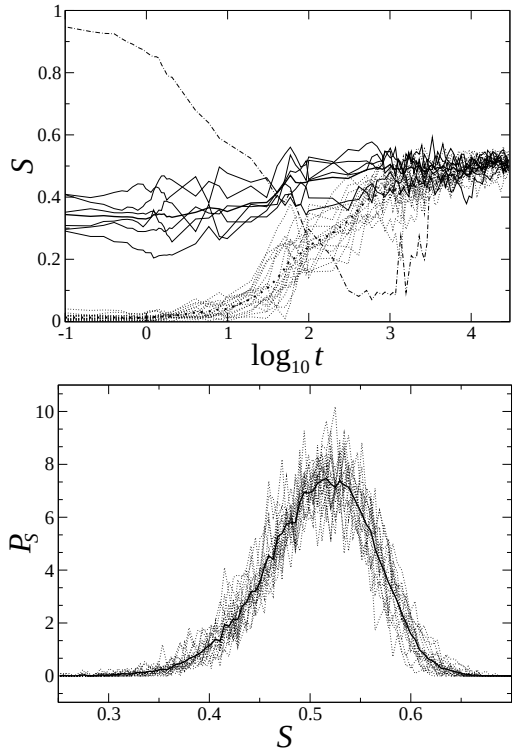

FIGURE 3

FIGURE 4

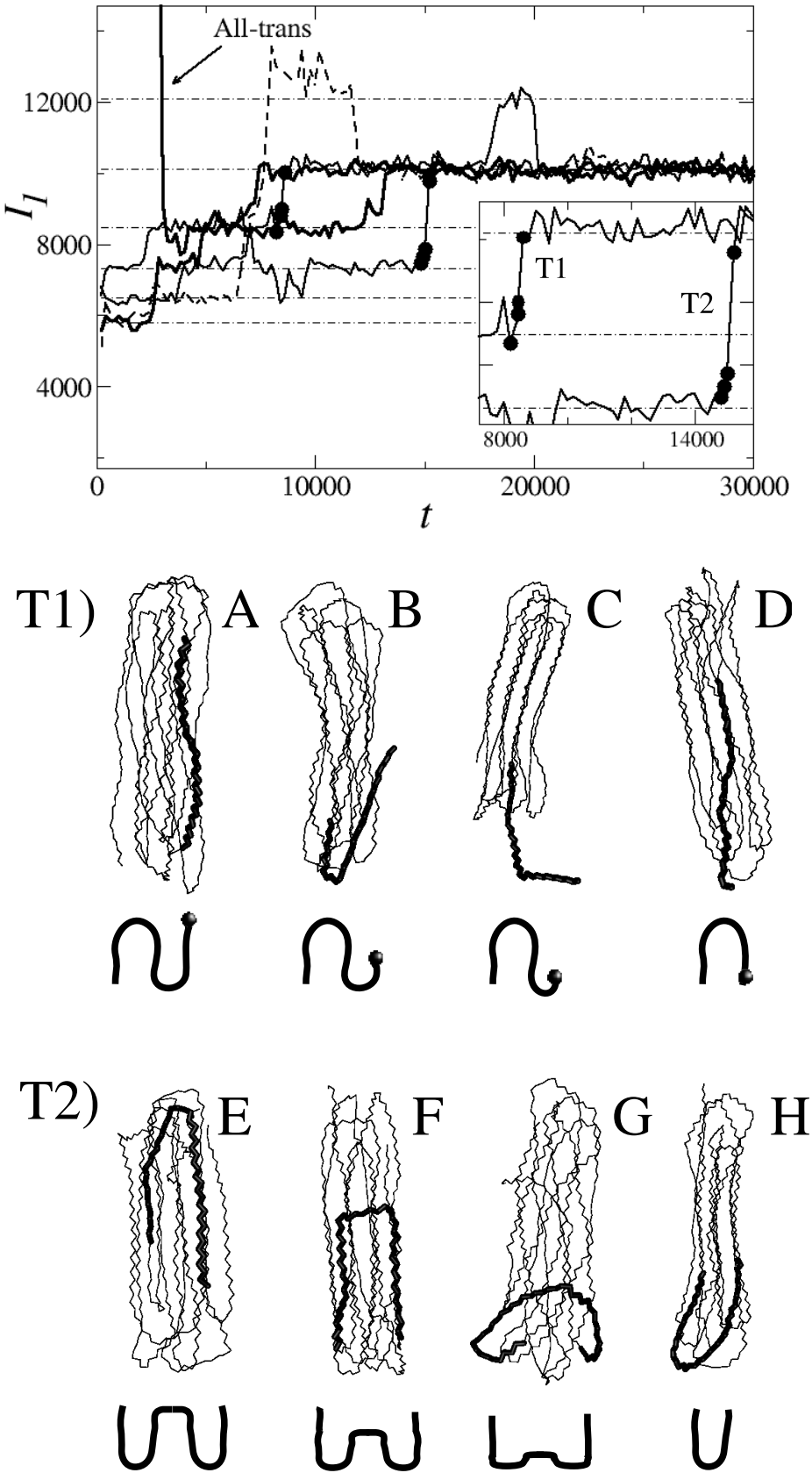
All-trans
12000
8000
4000
I_1
0
10000
20000
30000
t
T1
T2
8000
14000
T1)
A
B
C
D
T2)
E
F
G
H

FIGURE 5

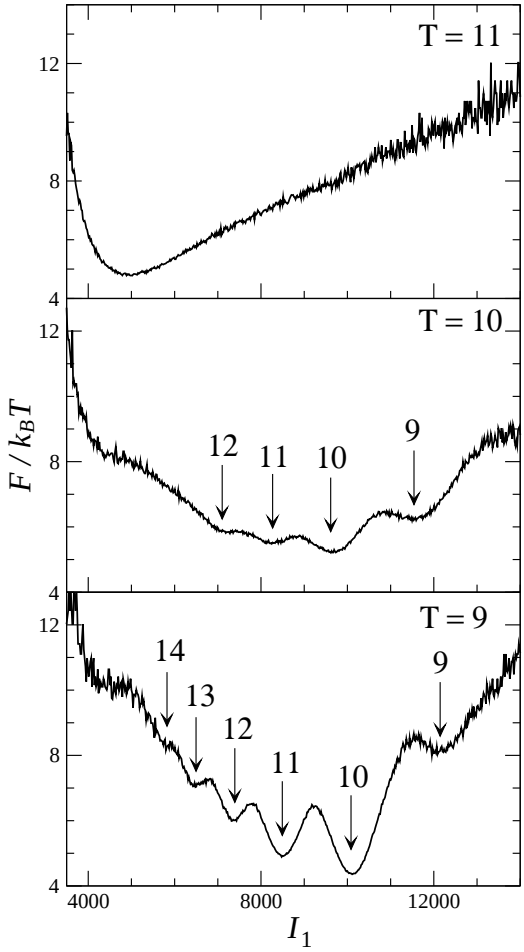

FIGURE 6

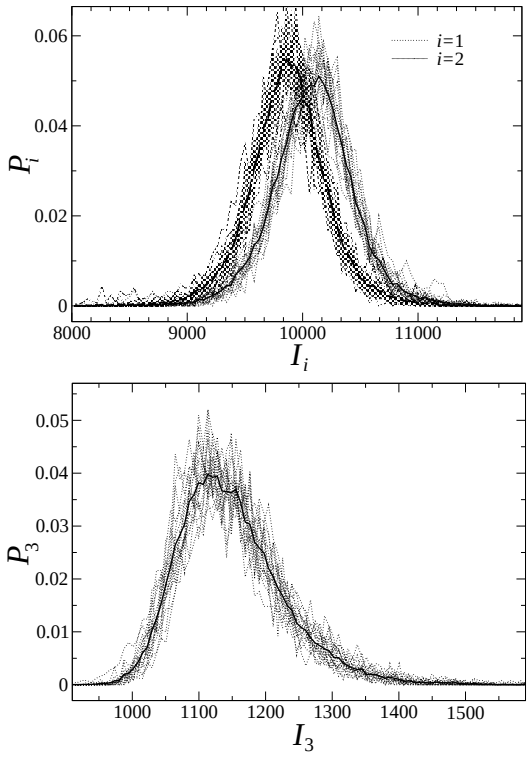
0.06
0.04
0.02
0
P_i
i=1
i=2
8000
9000
10000
11000
I_i
0.05
0.04
0.03
0.02
0.01
0
P_3
1000
1100
1200
1300
1400
1500
I_3

FIGURE 7

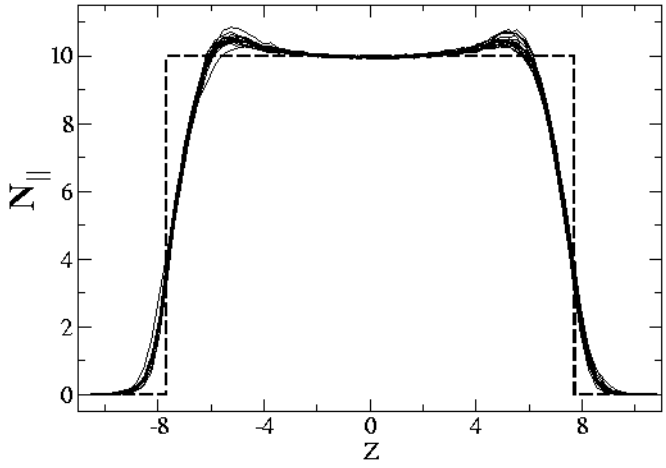

FIGURE 8

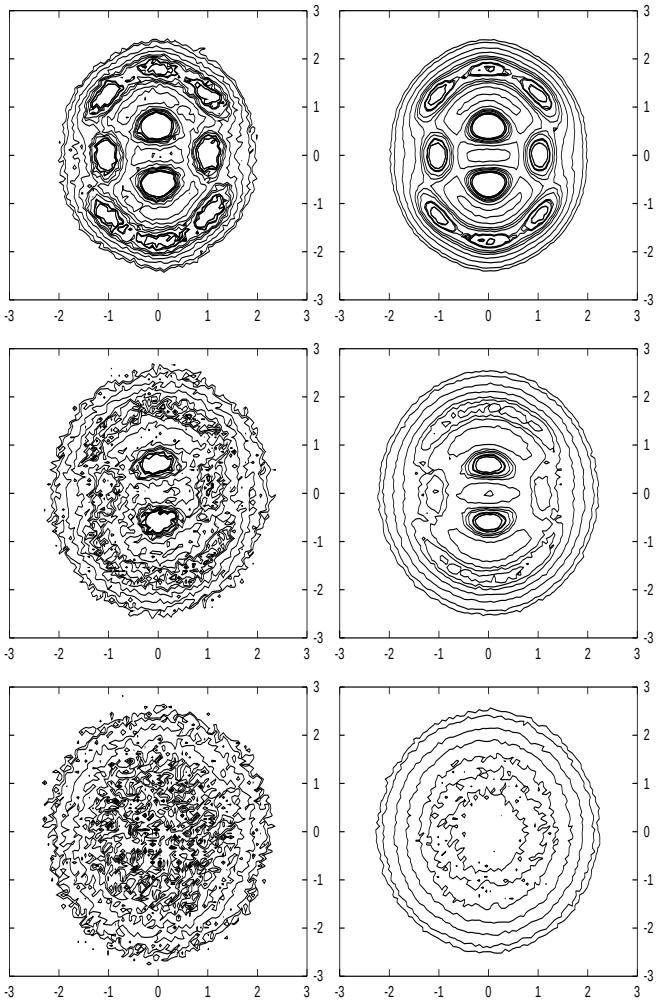

FIGURE 9

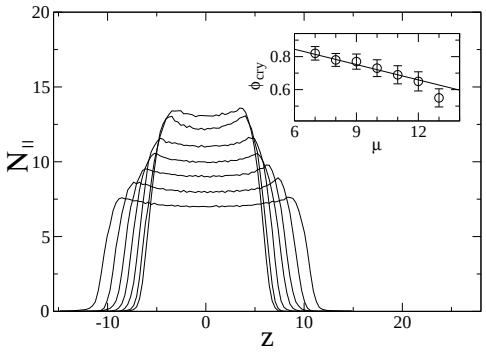

FIGURE 10

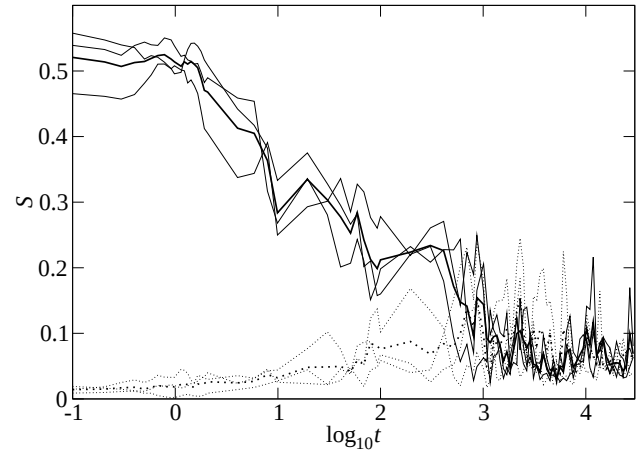
0.5
0.4
0.3
0.2
0.1
0
S
-1
0
1
2
3
4
log10t

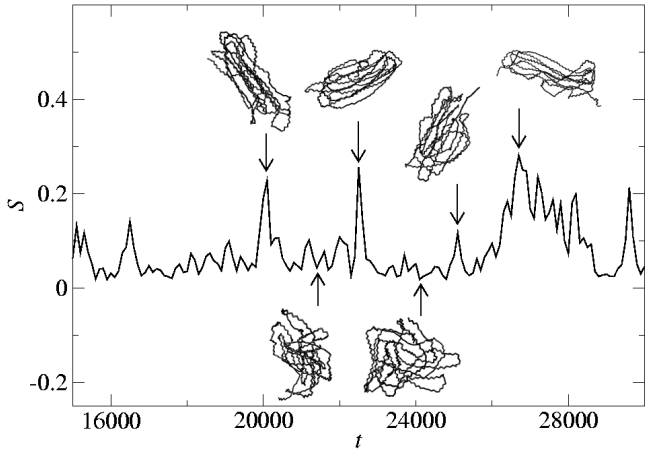
0.4
0.2
0
-0.2
S
16000
20000
24000
28000
t

FIGURE 11

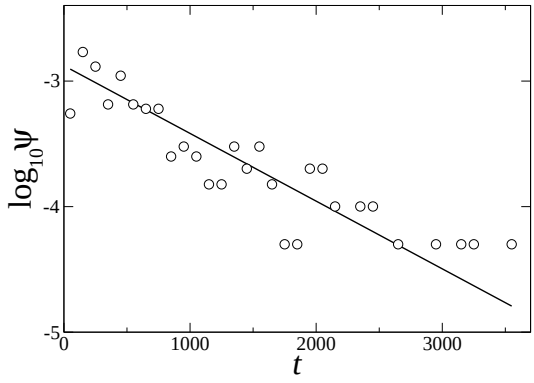

FIGURE 12